Mode selection in compressible active flow networks

Aden Forrow,[1] Francis G. Woodhouse,[2] and Jörn Dunkel[1,*]

[1] *Department of Mathematics, Massachusetts Institute of Technology, 77 Massachusetts Avenue, Cambridge MA 02139-4307, U.S.A.*

[2] *Department of Applied Mathematics and Theoretical Physics, Centre for Mathematical Sciences, University of Cambridge, Wilberforce Road, Cambridge CB3 0WA, U.K.*

(Dated: July 14, 2017)

Coherent, large scale dynamics in many nonequilibrium physical, biological, or information transport networks are driven by small-scale local energy input. Here, we introduce and explore an analytically tractable nonlinear model for compressible active flow networks. In contrast to thermally-driven systems, we find that active friction selects discrete states with a limited number of oscillation modes activated at distinct fixed amplitudes. Using perturbation theory, we systematically predict the stationary states of noisy networks and find good agreement with a Bayesian state estimation based on a hidden Markov model applied to simulated time series data. Our results suggest that the macroscopic response of active network structures, from actomyosin force networks to cytoplasmic flows, can be dominated by a significantly reduced number of modes, in contrast to energy equipartition in thermal equilibrium. The model is also well-suited to study topological sound modes and spectral band gaps in active matter.

PACS numbers: 47.63.-b, 05.70.Ln, 05.65.+b 05.40.-a

Active networks constitute an important class of nonequilibrium systems spanning a wide range of scales, from the intracellular cytoskeleton [1, 2] and amoeboid organisms [3–8] to macroscopic transport networks [9–12]. Identifying generic self-organization principles [13–15] that control the dynamics of these biological or artificial far-from-equilibrium systems remains one of the foremost challenges of modern statistical physics. Despite promising experimental [4–6, 16–18] and theoretical [1, 7, 19–21] advances over the past decade, it is not well understood how the interactions between local energy input, dissipation and network topology determine the coordinated global behaviors of cells [16], plasmodia [4–6] or tissues [22]. Further progress requires analytically tractable models that help clarify the underlying nonequilibrium mode selection principles [23, 24].

We in1998GaHaJuMatroduce here a generic model for active flows on a network, motivated by recent experimental studies of bacterial fluids [20, 25] and ATP-driven microtubule suspensions [26] in microfluidic channel systems. Building on Rayleigh's work [27] on driven vibrations and the Toner-Tu model of flocking [28], the theory accounts for network activity through a nonlinear friction [28–31]. We work in a fully compressible framework allowing accumulated matter at vertices to affect flow through network pressure gradients, generalizing previous work on incompressible pseudo-equilibrium active flow networks [32, 33], as suited to the many biological systems exhibiting flexible network geometry [4–6] or variations in the density of active components [15]. Although inherently nonlinear, the model can be systematically analyzed through perturbation theory. Such analysis shows how slow global dynamics emerge naturally from the fast local dynamics, enabling prediction of the typical states in large noisy networks; these states have significantly fewer active modes than for energy equipartition [34] in thermal equilibrium. More broadly, our model provides an accessible framework for investigating generic physical phenomena in active systems, including topologically-protected sound modes [15] and the influence of spectral band gaps (SM [35]).

We consider activity-driven mass flow on an arbitrarily-oriented graph $\mathbb{G} = (\mathcal{V}, \mathcal{E})$ with $V = |\mathcal{V}|$ vertices and $E = |\mathcal{E}|$ edges. The elements of the $V \times E$ gradient (incidence) matrix ∇ are $\nabla_{ve} = -1$ if edge e is oriented outwards from vertex v, $\nabla_{ve} = +1$ if e is oriented inwards into v, and $\nabla_{ve} = 0$ otherwise. The dynamical state variables are the deviations from the mean mass $\bar{\varrho} = M/V$ on the nodes, $(\varrho_1(t), \dots, \varrho_V(t))$, and the mass fluxes on the edges, $(\phi_1(t), \dots, \phi_E(t))$, governed by the non-dimensionalized (SM [35]) transport equations

$$\dot{\varrho}_v = \sum_e \nabla_{ve}\phi_e, \tag{1a}$$

$$\dot{\phi}_e = -\sum_v \nabla_{ev}^\top \varrho_v + \epsilon \frac{\mu - \phi_e^2}{1+\phi_e^2}\,\phi_e + \sqrt{2D}\xi_e(t), \tag{1b}$$

where $\xi_e(t)$ is standard Gaussian white noise. Equation (1a) ensures mass conservation. The first term on the r.h.s. of Eq. (1b) represents the gradient of an ideal gas-type node pressure $p_v \propto \varrho_v$, corresponding to the leading term in a virial expansion; the second term is a Toner-Tu type (SM [35]) active friction force derived from a depot model [29, 36] with coupling $\epsilon > 0$ and active–passive control parameter μ, which drives the edge fluxes ϕ_e towards preferred values $\pm\sqrt{\mu}$ when $\mu > 0$. Many networks have non-uniform edge and vertex weights, which can be incorporated into equations of identical form to Eqs. (1) with appropriate rescaling of ϱ, ϕ, and ∇ (SM [35]).

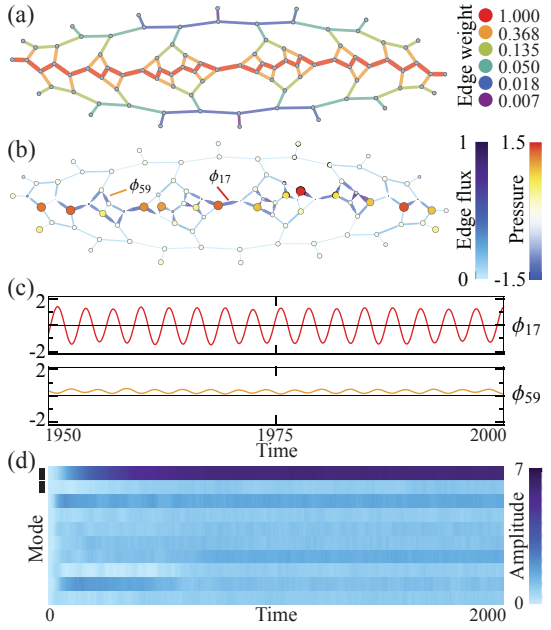

FIG. 1. Activity can select a single dominant oscillation mode on hierarchically weighted networks. (a) The edges in the graph simulated in (b) and (c) are given weights decreasing exponentially with their distance from the central red path. (b) Oscillations in pressure and flux develop primarily along the central high-weight path (Movie 1). (c) Edge fluxes ϕ_e settle into steady synchronized oscillations as exemplified for two edges indicated in (b), one on (ϕ_{17}) and one off (ϕ_{59}) the path. (d) Plotting the time-dependent amplitude of each analytically-determined flow eigenmode confirms selection of a single oscillatory mode. The ten modes with the highest average amplitude in this simulation run are pictured; the marked top two rows are oscillatory modes, while the remaining rows are cyclic modes. See Fig. S6 for all modes. Simulation parameters were $\epsilon = 0.1$, $\mu = 1$, and $D = 10^{-4}$.

Active flow networks described by Eqs. (1) exhibit rich oscillatory transport behavior, including the mode selection illustrated in Movie 1 and Fig. 1 for a hierarchically-weighted network with vertex degrees at most 3 as is typical of *Physarum polycephalum* [37]. When this network is initialized with zero pressure variation and flux, it typically settles into a quasi-steady state with a single dominant oscillation frequency on the highest-weight path. This is a manifestation of the fact that single-frequency selection is the norm on actively driven path graphs, as we shall show analytically below.

Generally, the features of the steady-state attractor will be determined by the topology of the subgraph of high-weight edges, which may be much sparser than the original network. For this reason, as well as for ease of analysis and illustration, we will henceforth assume $\mathbb{G}$ to be a tree, as realized in certain peripheral sensory neurons [38], though in general the full model in Eqs. (1) is not restricted to any particular class of graph. The behaviors observed on trees can be extended to denser graphs by choosing appropriate edge weights.

The complex active flow dynamics encoded by Eqs. (1) can be understood analytically by considering the basis of oscillation modes of the network, as we illustrate now in the fully deterministic case ($D = 0$). To progress, we adopt a Rayleigh [27] approximation $\epsilon(\mu - \phi_e^2)\phi_e$ for the active friction (SM [35]). Now, expand the pressure $\varrho_v = \sum_{n=1}^{E} r_n(t)\varrho_{vn}$ and flux $\phi_e = \sum_{n=1}^{E} f_n(t)\phi_{en}$ in the right and left singular vectors $\boldsymbol{\varrho}_n = (\varrho_{vn})$ and $\boldsymbol{\phi}_n = (\phi_{en})$ of $\nabla^\top$ corresponding to the $E = V - 1$ non-zero singular values λ_n. (On a tree, there is a single zero eigenvalue of $\nabla\nabla^\top$ yielding an additional right singular vector for the pressure, but this corresponds to a constant mass shift and so can be safely neglected.) Defining mode amplitudes $A_n^2 = r_n^2 + f_n^2$, the network energy then takes the simple form $H = \frac{1}{2}\sum_n \lambda_n^2 A_n^2$ (SM [35]). When ϵ is small there are two distinct timescales, namely the fast oscillation timescale t and the slow friction timescale $\tau = \epsilon t$, which we separate in the perturbation ansatz $r_n = \sum_{\sigma=0}^{\infty} \epsilon^\sigma r_{\sigma n}$ and $f_n = \sum_{\sigma=0}^{\infty} \epsilon^\sigma f_{\sigma n}$ [39]. Active friction does not contribute at lowest order, so the $O(1)$ contribution to each mode (r_n, f_n) is an uncoupled harmonic oscillator $r_{0n}(t) = A_{0n}(\tau)\cos[\lambda_n t - \delta_n(\tau)]$ and $f_{0n}(t) = -A_{0n}(\tau)\sin[\lambda_n t - \delta_n(\tau)]$ with t-independent amplitude A_{0n} and phase δ_n (SM [35]).

The influence of activity becomes apparent at first order in ϵ, introducing couplings between mode amplitudes whose dynamics encode the state selection behavior of the active network. Requiring that the $O(\epsilon)$ amplitudes r_{1n} and f_{1n} remain small relative to the leading terms implies that the secular (unbounded) terms in the first order equations must vanish [39]. Assuming negligible mode degeneracies, the slow dynamics of the $O(1)$ mode amplitudes $A_{0n}(\tau)$ are found to obey (SM [35])

$$\frac{d(A_{0n}^2)}{d\tau} = \left(\mu - \sum_{k=1}^{E} P_{nk} A_{0k}^2\right) A_{0n}^2, \tag{2}$$

where the overlap matrix $P_{nk} = \frac{3}{2}(1 - \frac{1}{2}\delta_{nk})\sum_e \phi_{en}^2\phi_{ek}^2$ encodes the network topology. Fixed points of Eq. (2) can then be found by choosing a subset of the A_{0n} to be zero and solving $\sum_{k=1}^{E} P_{nk}A_{0k}^2 = \mu$ for A_{0n}^2 over the remaining non-zero modes. If all the non-zero solutions for A_{0n}^2 are positive, then there is a stationary point with those modes activated (SM [35]).

Activity-driven fixed points with exactly one mode active always exist. If only mode p is active at leading order, then $A_{0n} = \sqrt{\mu/P_{pp}}\,\delta_{np}$ is a fixed point of Eq. (2). These amplitudes, which closely match both those calculated with the full unapproximated active friction force and those from averages computed over fully nonlinear simulations (SM [35]), show that as μ crosses 0 there is a supercritical Hopf bifurcation with $A_{0n} \sim \sqrt{\mu}$. However, the stability of such a single-mode state depends on topology: our simulations suggest that activity always selects exactly one oscillation mode in simple path graphs,

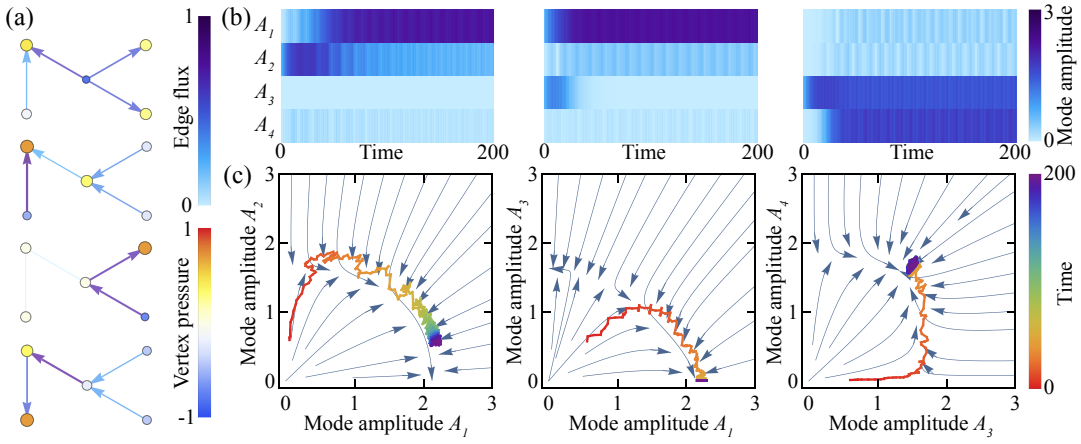

FIG. 2. First order perturbation theory accurately predicts the stable states on small trees. (a) A five vertex tree possessing four nontrivial modes, as illustrated. (b) On the tree in (a), mode amplitudes settle into one of two stable stationary states, as seen in simulations for three different initial conditions. Modes are ordered by frequency from high (top) to low (bottom). (c) Simulated mode trajectories (rainbow) in (b) match analytic predictions (blue streamlines) in the subspaces of activated modes. There are three possible arrangements of nonzero critical points in each 2D subspace: a saddle point on one axis and a stable node on the other axis (left), a stable node on each axis and a saddle point in the middle (center), or a saddle point on each axis and a stable node in the middle (right; Movie 2). Higher order effects cause both the convergence to a point with $A_2 > 0$ in the left and middle plots and the oscillations in the trajectories. Parameters used are $\epsilon = 0.5$, $\mu = 1$, $D = 0$.

whereas single-mode states are typically unstable in networks with complex topologies. We can use this observation to model more complex active networks with single mode selection by appropriately weighting the edges: if the edge weights for a path are large enough compared to the weights elsewhere in the network, the path behavior dominates (Fig. 1).

Insight into stability is provided by the case with up to two modes active. Writing $A_{0n} = A_{0p}\delta_{np} + A_{0q}\delta_{nq}$, Eq. (2) yields

$$d(A_{0p}^2)/d\tau = (\mu - P_{pp}A_{0p}^2 - P_{pq}A_{0q}^2)\,A_{0p}^2, \qquad (3)$$

and symmetrically for A_{0q}^2. Depending on the topology-encoding overlap coefficients P_{nk}, this gives up to four fixed points: the zero state $A_{0p} = A_{0q} = 0$, which is always linearly unstable; the single-mode state $(A_{0p}, A_{0q}) = (\sqrt{\mu/P_{pp}}, 0)$, which is stable if $P_{pq} > P_{pp}$ and a saddle if not, plus analogously for $(0, \sqrt{\mu/P_{qq}})$; and, potentially, a mixed state (A_{0p}^*, A_{0q}^*) where $A_{0p}^* = \sqrt{\mu\,(P_{qq} - P_{pq})/\left(P_{pp}P_{qq} - P_{pq}^2\right)}$ with A_{0q}^* defined symmetrically. When it exists, the mixed state is either stable (if $P_{pq}^2 < P_{pp}P_{qq}$) or a saddle (if $P_{pq}^2 > P_{pp}P_{qq}$), but if one of the single-mode states is stable and one is unstable, then one of A_{0p}^* and A_{0q}^* is imaginary and there is no mixed state. Hence, we have three possible scenarios (Fig. 2): one stable single mode and the other a saddle with no mixed state (Fig. 2b,c; left); two stable single-mode states with a mixed saddle in-between (Fig. 2b,c; center); and two single-mode saddles with a stable mixed state in-between (Fig. 2b,c; right). These predictions match simulations quantitatively even for relatively large ϵ beyond the small-ϵ perturbation regime (Fig. 2). In fact, simulations show the same qualitative behavior for $\epsilon = 2$, suggesting perturbation analysis remains predictive at high activity.

This two-mode analysis yields a simple topological heuristic for the stability of single-mode states. Since $|\boldsymbol{\phi}_p| = 1$, P_{pp} is small when $\boldsymbol{\phi}_p$ is spread over many edges and large when $\boldsymbol{\phi}_p$ is localized to a few edges. If $\boldsymbol{\phi}_q$ is localized to the same edges as $\boldsymbol{\phi}_p$, P_{pq} will also be large and mode p will be stable to perturbations in mode q. However, if $\boldsymbol{\phi}_q$ is localized to a disjoint set of edges, P_{pq} will be a scaled inner product of near-orthogonal vectors (ϕ_{ep}^2) and (ϕ_{eq}^2) and will be small. Thus localized modes will be unstable to modes in other regions, while conversely if a mode is to be stable alone then it will be spread out across the entire network. Therefore, a stable combination of modes will possess significant flows on all edges of the network.

Biological systems exhibit vastly different macroscopic and microscopic time scales [40–43]. This phenomenon is present in our compressible active flow network, where higher-order nonlinear effects induce slow global time scales from faster small-scale dynamics. When the zeroth-order amplitudes A_{0n} are at a fixed point, the first-order corrections r_{1n} and f_{1n} are harmonic oscillators with natural frequency λ_n driven at linear combinations of the frequencies active at zeroth order (SM [35]). For instance, if two modes p and q are active at zeroth order, the driving frequencies are $3\lambda_p - k(\lambda_p \pm \lambda_q)$ for $k = 0, \ldots, 3$. This introduces new, slower timescales into the dynamics, including oscillations in the energy $H = \frac{1}{2}\sum_n \lambda_n^2(r_n^2 + f_n^2)$ with frequency $\lambda_p - \lambda_q$. Their magnitude depends on the difference in frequency: slower

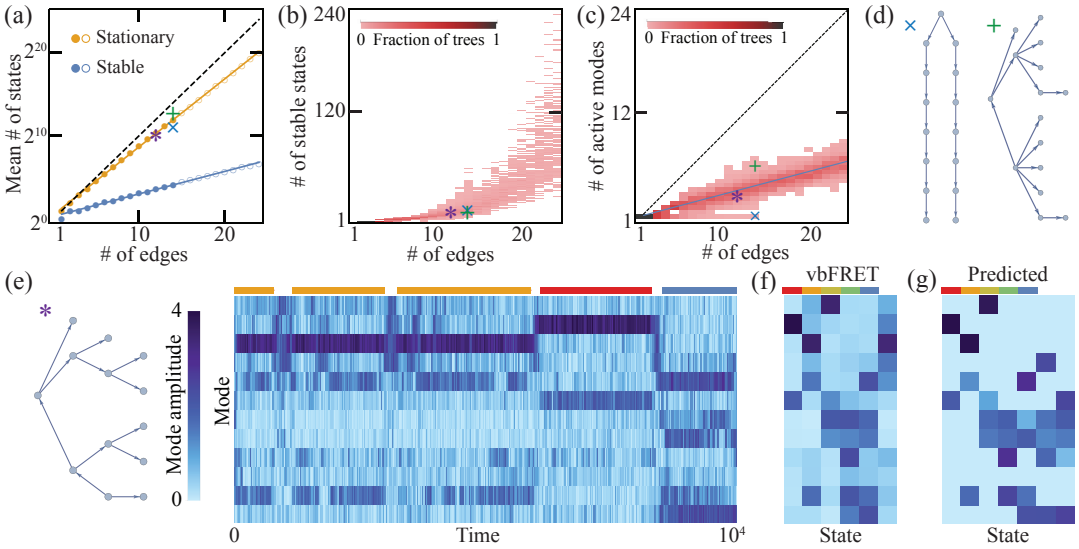

FIG. 3. States on larger trees possess surprisingly few active modes, which can be inferred from time series with non-zero noise. (a) The mean number of stationary states of Eq. (2) grows exponentially with edges E as $1.77^E \approx (2^E)^{4/5}$ (solid orange line), close to the upper bound of 2^E states (dashed black line), while the mean number of stable states grows as $1.21^E \approx (2^E)^{1/4}$ (solid blue line). We counted states on all nonisomorphic trees with $E \leq 14$ edges (filled circles) and on a random sample of ~ 175 trees per point for $15 \leq E \leq 24$ (open circles). Averages are over trees with a fixed number of edges. (b) As E increases, both the mean and the variance of the distribution of trees with each number of stable states increase rapidly. (c) Distribution of the average number of modes active in a stable state. The mean over trees scales like $0.26E \approx E/4$ (solid line), significantly below $E/2$ expected if modes were selected randomly. (d) Two example trees indicated in (a-c) by the corresponding colored symbols. Stable states on paths ($\times$) always only activate one mode; complex trees ($+$) have more modes active. (e) Noisy networks ($D > 0$) transition stochastically between stable states, exemplified by an amplitude-time trace for the tree shown. Modes are ordered by frequency from high (top) to low (bottom). Simulation parameters are $\epsilon = 0.5$, $\mu = 1$, $D = 5 \times 10^{-3}$. (f) States found by vbFRET from simulations on the tree in (e) (SM [35]). The second, first, and fifth columns are states seen in (e), indicated by the colored bars above. (g) States predicted by Eq. (2) for the tree in (e). The first five states in (f) match those in (g); the sixth column in (f) is likely a transient combination of analytically stable states.

oscillations, driven by modes with similar frequencies $\lambda_p \approx \lambda_q$, have higher amplitudes (SM [35], Fig. S7).

The number of activated modes in an arbitrary compressible active network depends on intricate interactions between local activity and global flow configurations. The total number of available modes is equal to the number of edges E, meaning that, were each combination of modes to be a fixed point, a tree could have up to 2^E stationary states. To see how the true number of stationary and stable states depends on tree size, we performed an exhaustive numerical fixed point search of Eq. (2) over a large sample of trees with $E \leq 24$ (Fig. 3a-d). The naive upper bound of 2^E suggests exponential growth of the mean number of steady states with edges E; this is indeed what we see, going as $\sim (2^E)^{4/5}$. However, though still exponential in E, the mean number of stable states is much smaller at $\sim (2^E)^{1/4}$ (Fig. 3a). Remarkably, these stable states have only $\sim E/4$ modes active on average (Fig. 3c) in stark contrast to the activation of all E modes under thermal equipartition [34]. Path-like topologies lead to even more dramatic reductions in the number of modes active (Fig. 3c), suggesting that a biological system can further reduce the number of active modes through an optimal choice of topology; moreover, hierarchically tuned edge capacities as realized in *Physarum* [5, 6, 37] can further enhance mode selection even in non-tree topologies (Fig. 1).

Real active transport networks will have some nonzero level of thermal or athermal noise [44–46]. Provided the noise is not too large, it will render previously stable states now only metastable, with flow patterns exhibiting small fluctuations around these metastable states punctuated by noise-driven stochastic transitions between them [32, 46]. Long-time simulations of Eqs. (1) with $D > 0$ therefore offer an independent numerical way to find stable fixed points of the amplitude dynamics. We use vbFRET [47], a variational Bayesian analysis of a continuous time hidden Markov model, to identify states from simulated time series. Almost all of the states discovered by vbFRET match stable states predicted by Eq. (2) even in the presence of non-negligible noise (Fig. 3e-g), justifying the simplifications used in deriving Eq. (2). This also promises that Bayesian methods like vbFRET will function as reliable inference tools for experimental data from real-life active flow networks [4, 5, 18].

Beyond active density oscillations [20], the above theoretical framework can be used to probe the effects of topology on the physical properties of complex active systems. For instance, it was recently shown that continuum Toner–Tu systems in finite lattice confinement possess topologically protected edge-localized sound modes [15]. Similar edge modes can be reproduced in our coarse-grained model through a simplified network representation of complex channel geometries (SM [35] and Movie 3). In addition, generalizing to allow different effective weights at vertices opens up band gaps, reflected in the excitation spectrum of spontaneous activity modes (SM [35]). As we focus on phenomenological properties shared by many active systems, akin to the Toner–Tu approach [28], the results and techniques presented here promise insights into the mode selection mechanisms governing a wide range of non-equilibrium transport and force networks.

This work was supported by NSF Award CBET-1510768 (A.F. and J.D.), Trinity College, Cambridge (F.G.W.), and an Alfred P. Sloan Research Fellowship (J.D.). The authors thank Martin Zwierlein for stimulating discussions on band gaps.

* dunkel@mit.edu

[1] C. Broedersz and F. MacKintosh, Rev. Mod. Phys. **86**, 995 (2014).

[2] V. Ruprecht, S. Wieser, A. Callan-Jones, M. Smutny, H. Morita, K. Sako, V. Barone, M. Ritsch-Marte, M. Sixt, R. Voituriez, and C.-P. Heisenberg, Cell **160**, 673 (2015).

[3] A. Takamatsu, R. Tanaka, H. Yamada, T. Nakagaki, T. Fujii, and I. Endo, Phys. Rev. Lett. **87**, 7 (2001).

[4] A. Tero, S. Takagi, T. Saigusa, K. Ito, D. P. Bebber, M. D. Fricker, K. Yumiki, R. Kobayashi, and T. Nakagaki, Science **327**, 439 (2010).

[5] K. Alim, G. Amselem, M. P. Brenner, and A. Pringle, Proc. Natl. Acad. Sci. U.S.A. **110**, 13306 (2013).

[6] K. Alim, N. Andrew, A. Pringle, and M. P. Brenner, Proc. Natl. Acad. Sci. USA **114**, 5136 (2017).

[7] V. Bonifaci, K. Mehlhorn, and G. Varma, J. Theor. Biol. **309**, 121 (2012).

[8] C. R. Reid, H. Macdonald, R. P. Mann, J. A. R. Marshall, T. Latty, and S. Garnier, J. R. Soc. Interface **13**, 44 (2016).

[9] G. Coclite, M. Garavello, and B. Piccoli, SIAM J. Math. Anal. **36**, 1862 (2005).

[10] B. Piccoli and M. Garavello, *Traffic Flow on Networks: Conservation Laws Models* (AIMS, Springfield, MO, 2006).

[11] S. Hata, H. Nakao, and A. S. Mikhailov, Phys. Rev. E **89**, 020801 (2014).

[12] L. L. Heaton, E. López, P. K. Maini, M. D. Fricker, and N. S. Jones, Phys. Rev. E **86**, 021905 (2012).

[13] H. Nakao and A. S. Mikhailov, Nat. Phys. **6**, 544 (2010).

[14] A. S. Mikhailov and K. Showalter, Chaos **18**, 026101 (2008).

[15] A. Souslov, B. C. van Zuiden, D. Bartolo, and V. Vitelli, arXiv:1610.06873.

[16] N. Fakhri, A. D. Wessel, C. Willms, M. Pasquali, D. R. Klopfenstein, F. C. MacKintosh, and C. F. Schmidt, Science **344**, 1031 (2014).

[17] P. Ronceray, C. P. Broedersz, and M. Lenz, Proc. Natl. Acad. Sci. U.S.A. **113**, 2827 (2016).

[18] S. Marbach, K. Alim, N. Andrew, A. Pringle, and M. P. Brenner, Phys. Rev. Lett. **117** (2016).

[19] C. P. Broedersz, X. Mao, T. C. Lubensky, and F. C. MacKintosh, Nat. Phys. **7**, 983 (2011).

[20] M. Paoluzzi, R. Di Leonardo, and L. Angelani, Phys. Rev. Lett. **115**, 188303 (2015).

[21] A. Bressan, S. Canić, M. Garavello, M. Herty, and B. Piccoli, EMS Surv. Math. Sci. **1**, 47 (2014).

[22] C. G. Vasquez and A. C. Martin, Dev. Dynam. **245**, 361 (2016).

[23] W. Ebeling, U. Erdmann, J. Dunkel, and M. Jenssen, J. Stat. Phys. **101**, 443 (2000).

[24] J. Dunkel, W. Ebeling, U. Erdmann, and V. A. Makarov, Int. J. Bifurcat. Chaos **12**, 2359 (2002).

[25] H. Wioland, E. Lushi, and R. E. Goldstein, New J. Phys. **18**, 075002 (2016).

[26] K.-T. Wu, J. B. Hishamunda, D. T. N. Chen, S. J. DeCamp, Y.-W. Chang, A. Fernández-Nieves, S. Fraden, and Z. Dogic, Science **355**, eaal1979 (2017).

[27] J. W. S. B. Rayleigh, *The Theory of Sound vol. 1*, 2nd ed. (Macmillan, New York, 1894) p. 81.

[28] J. Toner, Y. Tu, and S. Ramaswamy, Annals of Physics **318**, 170 (2005).

[29] F. Schweitzer, W. Ebeling, and B. Tilch, Phys. Rev. Lett. **80**, 5044 (1998).

[30] P. Romanczuk, M. Bär, W. Ebeling, B. Lindner, and L. Schimansky-Geier, Eur. Phys. J. Spec. Top. **202**, 1 (2012).

[31] P. S. Burada and B. Lindner, Phys. Rev. E **85**, 032102 (2013).

[32] F. G. Woodhouse, A. Forrow, J. B. Fawcett, and J. Dunkel, Proc. Natl. Acad. Sci. U.S.A. **113**, 8200 (2016).

[33] F. G. Woodhouse and J. Dunkel, Nat. Commun. **8**, 15169 (2017).

[34] A. I. Khinchin, *Mathematical Foundations of Statistical Mechanics* (Dover, New York, 1949).

[35] See Supplemental Material, which includes Refs. [48].

[36] P. Romanczuk, W. Ebeling, U. Erdmann, and L. Schimansky-Geier, Chaos **21**, 047517 (2011).

[37] W. Baumgarten, T. Ueda, and M. J. B. Hauser, Phys. Rev. E **82**, 046113 (2010).

[38] J. Kromer, A. Khaledi-Nasab, L. Schimansky-Geier, and A. B. Neiman, ArXiv:1701.01693.

[39] S. H. Strogatz, *Nonlinear Dynamics and Chaos* (Westview Press, Boulder, CO, 2015).

[40] J. Halatek and E. Frey, Cell Rep. **1**, 741 (2012).

[41] R. A. Kerr, H. Levine, T. J. Sejnowski, and W. Rappel, Proc. Natl. Acad. Sci. U.S.A. **103**, 347 (2006).

[42] I. H. Riedel-Kruse, C. Müller, and A. C. Oates, Science **317**, 1911 (2007).

[43] A. Varma, K. C. Huang, and K. D. Young, J. Bacteriol. **190**, 2106 (2008).

[44] B. Lindner, J. Garcıa-Ojalvo, A. Neiman, and L. Schimansky-Geier, Phys. Rep. **392**, 321 (2004).

[45] L. Gammaitoni, P. Hänggi, P. Jung, and F. Marchesoni, Rev. Mod. Phys. **70**, 223 (1998).

[46] P. Hänggi, P. Talkner, and M. Borkovec, Rev. Mod.

Phys. **62**, 251 (1990).
[47] J. E. Bronson, J. Fei, J. M. Hofman, R. L. Gonzalez, and C. H. Wiggins, Biophys. J. **97**, 3196 (2009).
[48] J. W. S. B. Rayleigh, Proc. Lond. Math. Soc. **s1-10**, 4 (1878); P. Misra, *Physics of Condensed Matter* (Elsevier Science, 2011).